J. COMBIN. MATH. COMBIN. COMPUT. 127b (2025) 8467--8483

Journal of Combinatorial Mathematics and Combinatorial Computing
www.combinatorialpress.com/jcmcc

Research and development of VSC power disturbance generator

Zheng Na[1,✉], Dantian Zhong[1], Xuejie Wang[1], Zhichao Wen[2], Yang You[2], Yixuan Wang[1]

[1] *School of Electric Power, Shenyang Institute of Technology, Shenyang, Liaoning, 110000, China*

[2] *Panjin Power Supply Company, State Grid Liaoning Electric Power Co., Ltd., Panjin, Liaoning, 124000, China*

ABSTRACT

In order to provide various disturbance voltage waveforms for the test of power quality event detection and compensation device, it is necessary to develop a device that can simulate power grid faults. VSC power disturbances generator (VSC-IG, Interruption Generator based on Voltage Source Converter) is the importance of theoretical study and compensation device of power quality test tools, the flexibility to produce all kinds of disturbance voltage waveform, And reduce the harmonic pollution to the power grid. In this paper, the power injected by AC power supply into VSC-IG is controlled to stabilize the DC voltage, and a PI controller parameter tuning method considering the change of resistance parameters is proposed to optimize the dynamic performance of the controller. The SPWM rule sampling method is adopted as the underlying control strategy to realize the generation of disturbance voltage waveform. PSCAD/EMTDC platform is used to build the VSC-IG simulation model and carry out the simulation research. The VSC-IG device is designed and implemented by using the physical prototype hardware platform of 30kVA back-to-back converter in dynamic modeling laboratory. The experiment verifies the main circuit structure and control strategy of VSC-IG in this paper, and also verifies the function of digital controller, which lays a foundation for further research on power quality.

Keywords: voltage converter; Disturbance generator; Feedback linearization; Power control; Regular sampling

1. Introduction

Voltage source converter (VSC) is a key device used in high-voltage direct current (HVDC) systems, which realizes the conversion of AC and DC by converting AC to DC and has the ability of reactive power regulation [1-3]. The VSC plays an important role in the conversion, transmission, and control

✉ Corresponding author.
E-mail address: 76352648@163.com (Z. Na).
Received 05 March 2024; Revised 10 May 2024; Accepted 05 December 2024; Published Online 16 April 2025.
DOI: 10.61091/jcmcc127b-463

of electric power in power systems, and is of great significance in realizing the high efficiency, flexibility, and reliability of power transmission.

VSC connects a group of power semiconductor devices in series at the input, and realizes the control of input alternating current by controlling the switching state of these devices [4-5]. Through appropriate switching control, VSC can realize the frequency and amplitude adjustment of AC power, so as to realize the precise control of DC power [6-7]. VSC has various applications in HVDC system. The most common ones are bi-directional converter which can realize bi-directional energy transfer, and multi-terminal DC system formed by connecting multiple VSCs together [8-10]. Compared with the traditional converter technology, VSC has many advantages. Firstly, VSCs have the ability to regulate reactive power without the need for synchronous mechanical devices and can be started without an external power supply [11-12]. Secondly, the use of power semiconductor devices for switching control results in faster commutation, higher reliability, and reduced need for mechanical components [13]. Despite the many advantages of VSC, it also suffers from problems of cost and electromagnetic compatibility. In large-scale applications VSC requires a large number of power semiconductor devices, which are costly, while high-frequency switching operations may cause electromagnetic interference [14-16]. In addition, the control algorithms and protection mechanisms of VSCs are also the focus of research. VSCs can control the active and reactive power on the AC side, and the power control is important to realize the flexible conversion and transmission of electric energy [17-19]. The disturbance can observe the functional control to stabilize the realization of AC and DC conversion.

VSC has an important position in the modern energy system and is widely used in large-scale wind power generation, offshore wind power, long-distance transmission and other fields [20-22]. With the rapid development of renewable energy and the improvement of energy transmission efficiency and stability requirements of power systems, VSC will be more widely used. In the future, VSC will pay more attention to the development of high efficiency, reliability and intelligence. Meanwhile, with the continuous breakthrough and innovation of key technologies such as power semiconductor devices and control algorithms, VSC will further improve its performance.

In this paper, type selection of voltage source converter (VSC) as the research object, constructing VSC type power disturbances generator (Interruption Generator Based on Voltage Source Converter, VSC-IG). VSC-IG converts industrial AC power into DC voltage, and uses PWM technology to control the output voltage of the inverter side to realize the disturbance voltage waveform.

2. Controller design of 1VSC-IG

2.1. *Feedback linear decoupling control design*

The control goal of the VSC power disturbance generator is to realize the fixed DC voltage by the grid-side converter. The load side converter realizes the generation of the specified disturbance voltage waveform. Let the output variable be $Y_1 = h_1(X) = i_d$, $Y_2 = h_2(X) = i_q$. The outcome is an affine nonlinear system with dual inputs and dual outputs.

$$\begin{cases} \dot{X} = f(X) + g_1(X)u_1 + g_2(X)u_2 \\ Y_1 = h_1(X) \\ Y_2 = h_2(X) \end{cases} \tag{1}$$

Formula: $f(X) = \begin{pmatrix} \dfrac{E_{sd} - Rx_1}{L} + \omega x_2 \\ \dfrac{-Rx_2}{L} - \omega x_1 \end{pmatrix}$, $g_1(x) = \begin{pmatrix} -\dfrac{u_{dc}}{L} \\ 0 \end{pmatrix}$, $g_2(x) = \begin{pmatrix} 0 \\ -\dfrac{u_{dc}}{L} \end{pmatrix}$.

2.2. Controller performance optimization

Figure 1 illustrates the dynamic configuration of the current loop control system.

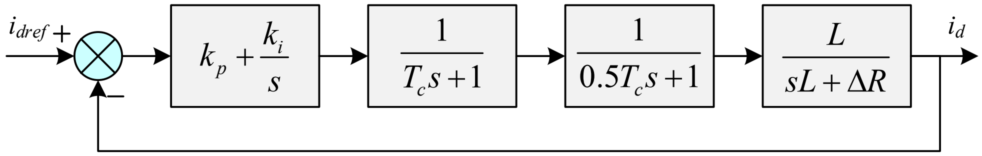

Fig. 1. The control system's dynamic framework during variations in resistance

The characteristic function in the open-loop configuration of the system is defined as

$$G_{id}(s) = \frac{k_p s + k_i}{s} \bullet \frac{1}{0.5T_c^2 s^2 + 1.5T_c s + 1} \bullet \frac{L}{Ls + \Delta R} \tag{2}$$

The PI controller's nullifying zero is neutralized by the pole that arises due to the disturbance of resistance parameter. The open-loop transfer function, having undergone correction, now stands as

$$G_{id}(s) = \frac{k_p}{s(1.5T_c s + 1)} \tag{3}$$

Under steady state conditions, E_{sd} is a constant value, and On the direct current side, the voltage and current are set by the load characteristics. Therefore, the premise of ensuring the constant DC voltage is the constant i_d . Add a voltage ring to the outside of the current ring and use a PI controller to correct it, so that the benchmark of the i_d of the DC voltage deviation can be obtained through the PI link:

$$i_{dref} = (k_{vp} + \frac{k_{vi}}{s})(U_{dcref} - U_{dc}) \tag{4}$$

Where: k_{vp} and k_{vi} are the proportional gain factor and differential gain factor of the voltage loop PI regulatory system respectively.

Considering the delay of DC voltage signal sampling, the dynamic structure schematic representation of DC voltage regulation is as follows (Figure 2~ Figure 3):

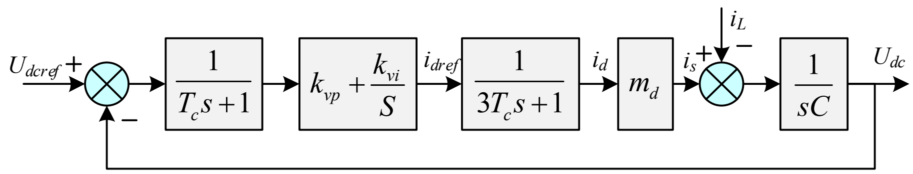

Fig. 2. Dynamic structure of DC voltage control

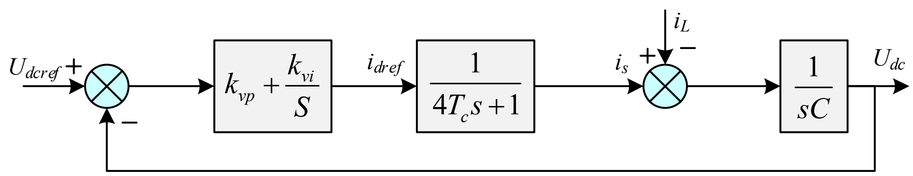

Fig. 3. Simplified dynamic structure diagram of voltage loop control system

Based on the properties of the switching mechanism, m_d in the structure diagram is a relationship that deviates from linearity, so it brings inconvenience to the configuration strategy for the system. Here, because m_d is a modulation ratio, when SPWM modulation is adopted, the upper limit of m_d is 1, and when md is the maximum value, it plays the most crucial role in shaping the system's dynamics. so it is reasonable to carry out this approximate treatment on the system. By combining the delayed items and ignoring the higher-order items, a simplified schematic of the system's dynamics is depicted in the accompanying figure.

Based on Mason's formula, the system's transfer function can be determined as

$$u_{dc}(s)=\frac{k_{vp}s+k_{vi}}{4CT_c s^3+Cs^2+k_{vp}s+k_{vi}}\cdot u_{dcref}(s)-\frac{4T_c s^2+s}{4CT_c s^3+Cs^2+k_{vp}s+k_{vi}}\cdot i_L(s) \tag{5}$$

The error in the system's steady-state operation is immune to the effects of load-induced interference currents, and the steady-state characteristics are good. The formulation of the system's equation is straightforward and can be outlined as follows:

$$(s^2+2\xi\omega_n s+\omega_n^2)(s+n\xi\omega_n)=0 \tag{6}$$

After the voltage loop PI controller is adjusted, the parameters are

$$\begin{cases} k_{vp}=4CT_c(2n\xi^2+1)\omega_n^2 \\ k_{vi}=4CT_c n\xi\omega_n^3 \end{cases} \tag{7}$$

Among them: $\omega_n=\frac{1}{4\xi T_c(n+2)}$.

3. VSC-IG computer numerical simulation research

To affirm the accuracy of the controller's design and main circuit parameters designed in this paper and to study the work of VSC-IG, a VSC-IG simulation research platform with a capacity of 30kVA was built on PSCAD/EMTDC simulation software. Figure 4 illustrates the simulation research platform developed using PSCAD software. On the simulation research platform, the performance of the controller and the dynamic response of the system can be evaluated comprehensively by setting various operating parameters. The simulation results show that the designed controller can effectively adjust the output voltage and current of VSC-IG to ensure its stability and reliability under different load and operating conditions. At the same time, by comparing the simulation data under different control strategies, the control parameters can be further optimized to improve the robustness and immunity of the system. According to the discussion of the parameter design of controller and main circuit in this paper, after comprehensive measurement and debugging, the PI parameters of controller and main circuit parameters of device are selected as shown in Table 1 and Table 2 respectively.

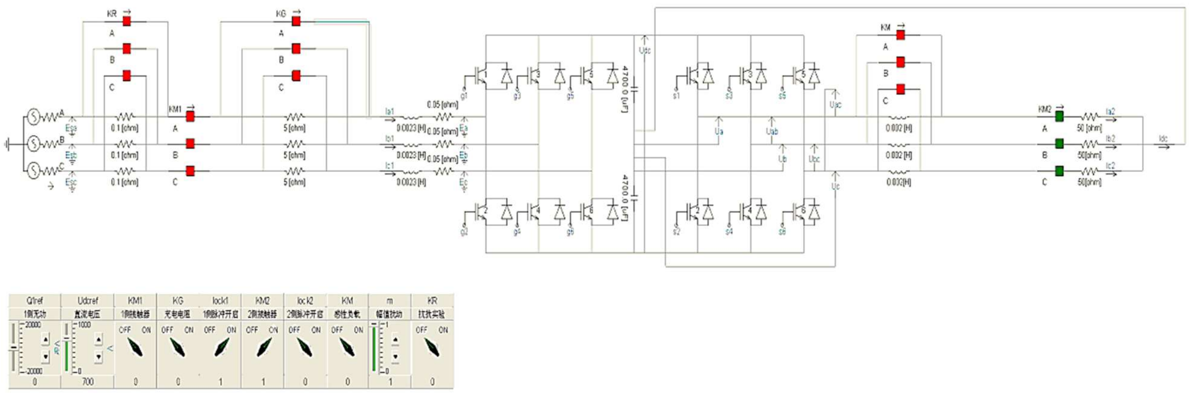

Fig. 4. PSCAD software simulation diagram

Table 1. The PI controller's parameters

Current loop PI parameter		Voltage loop PI parameter	
kp	Ti	kvp	Tvi
1400	0.00089s	0.6	0.02s

Table 2. Main circuit parameters of the device

Main circuit parameter	Numerical value
Voltage of a single phase in alternating current power supply/V	220
Grid side reactor/mH	2.3
Equivalent loss resistance /Ω	0.05
Dc equivalent capacitance/μF	7050
Dc capacitor operating voltage/V	700
Operating switching frequency/kHz	4

3.1. Power control operation simulation

Firstly, the controller characteristics of the designed network-side converter are verified (see Figure 5).

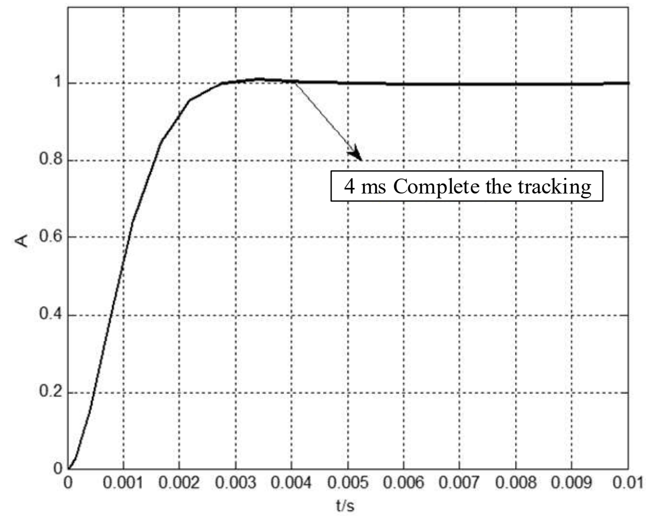

a) Current response curve

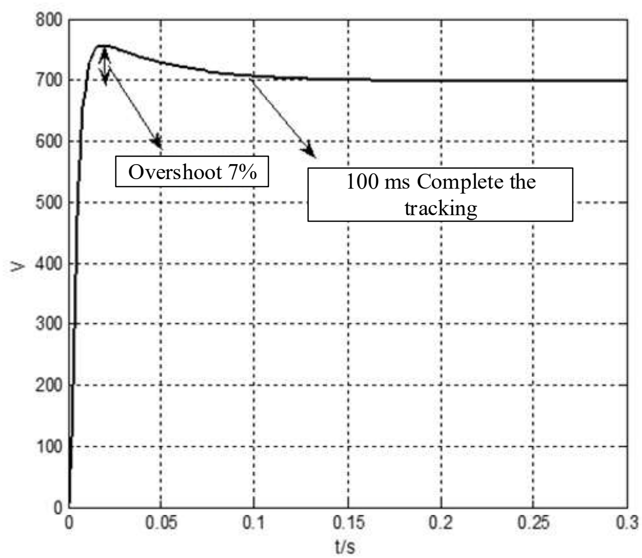

b) Dc voltage response curve

Fig. 5. Output response curve of double closed loop control system

It can be seen that the current can be tracked after 4ms, the control system is characterized by a small initial peak in response, followed by a stable operation with no persistent deviation from the setpoint. The working performance of the current loop control system is good. The results show that it proves to be a feasible strategy to utilize the zero pole cancellation method to track and control the dq axis current. The DC side voltage eventually converges to its steady-state magnitude 700V after 100ms, and there is no static difference attaining steady-state conditions, and the system exhibits an overshoot of 7%. The transient and steady-state performance are good. The results verify the correctness of the design of voltage loop controller. Further analysis shows that the current loop control system has excellent performance in both dynamic response and steady-state accuracy. In terms of dynamic response, the current can be tracked within 4ms, indicating that the system has a fast response speed and a small time constant, which is particularly important for current regulation under transient conditions. The low overshoot reflects the good stability of the system and avoids the problem of current fluctuation due to excessive transient response. The steady-state no static difference indicates that the controller can accurately track the set value and keep the current at the target value to achieve high precision control.

For the DC side voltage, the simulation results show that it reaches the steady-state value 700V within 100ms, with no static error and 7% overshoot, which indicates that the system also has good performance in voltage regulation. The adjustment time of 100ms indicates that the system can adapt to load changes and input voltage fluctuations quickly, and ensure the stability of DC voltage. An overshoot of 7% is an acceptable range in power electronic systems, indicating that the system can avoid excessive voltage fluctuations during regulation and ensure stable operation. The results verify the correctness of the design of voltage loop controller.

3.2. Simulation of disturbance voltage control

To initially grasp the properties of the waveform emitted by the disturbance device, so as to facilitate the debugging of relevant parameters in the actual device, the computer simulation of the disturbance waveform emitted by the device is carried out in this section, and the generation of the following disturbance voltages is realized.

1) Voltage drop within 0.2s~0.3s, the amplitude of control A phase voltage U_a decreases from 311V to 245V, and then returns to the original amplitude. The simulation waveform of the output waveform after filtering by the filter module in the PSCAD simulation environment is shown in Figure 6.

2) When the voltage rises temporarily from 0.2s to 0.3s, the amplitude of the control A phase voltage Ua increases from 311V to 350V, and then returns to the original amplitude. The filtered simulation waveform is shown in Figure 7.

3) Controlling the phase voltage's output pulse switch is a method used to achieve voltage interruption, and the pulse is blocked within 0.2s~0.3s, and then the pulse is turned on. The simulation waveform obtained with voltage interruption of 100ms is shown in Figure 8.

4) Frequency offset By changing the modulation wave frequency to 49Hz and 51Hz, the output simulation waveform is obtained, as shown in Figure 9 and Figure 10 respectively.

5) Harmonic injection Superimposes the fundamental voltage and the third harmonic voltage of 50% of its amplitude, and the simulation waveform after the third harmonic injection is shown in Figure 11. Its voltage spectrum is shown in Figure 12, from which the frequency distribution of the output voltage can be clearly seen, and the frequency spectrum is mainly distributed in the fundamental wave and the third harmonic frequency band.

6) Three-phase unbalance control Three-phase phase voltage Ua, Ub, Uc are of different amplitudes, and the waveform of three-phase unbalance voltage is shown in Figure 13. The unbalance of three-phase voltage is 32.5%. The simulation results verify the feasibility of VSC-IG development.

The simulation results are basically consistent with the theory, and the design scheme can effectively guide the development of the physical device.

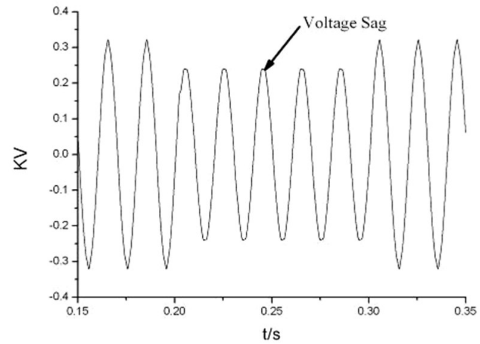

Fig. 6. Simulation waveform of voltage dip

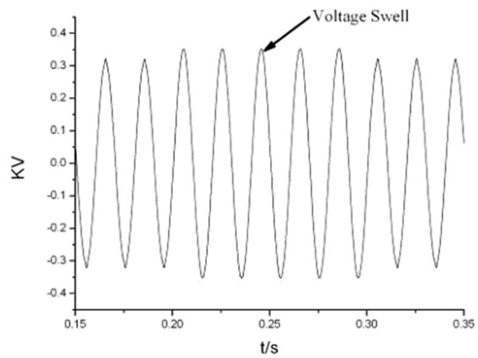

Fig. 7. Simulation waveform of voltage temporary rise

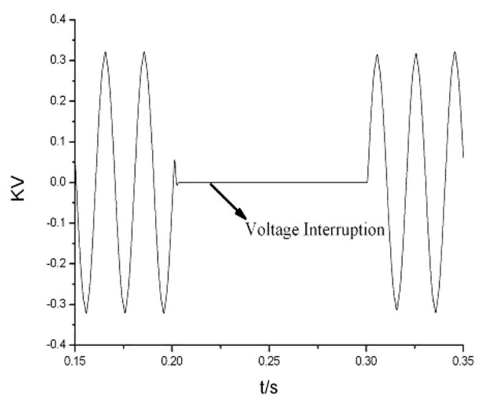

Fig. 8. Voltage interruption simulation waveform

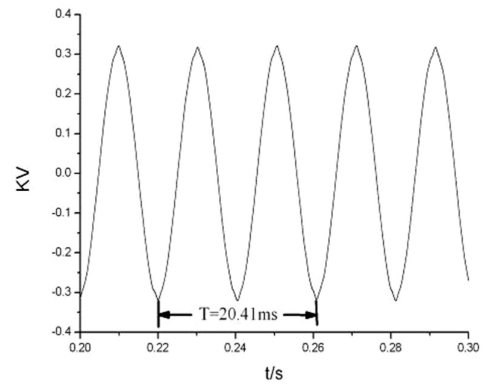

Fig. 9. 49Hz frequency waveform

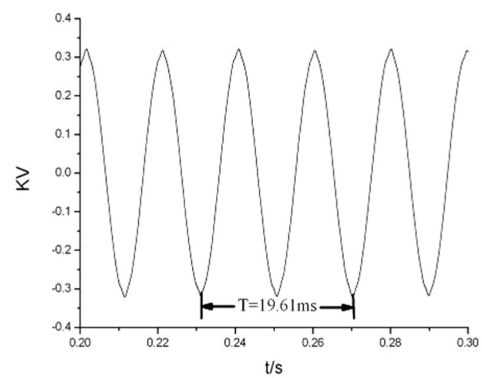

Fig. 10. 51Hz frequency waveform

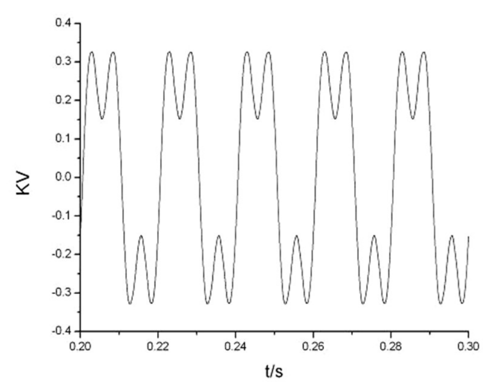

Fig. 11. Waveform diagram of injected third harmonics

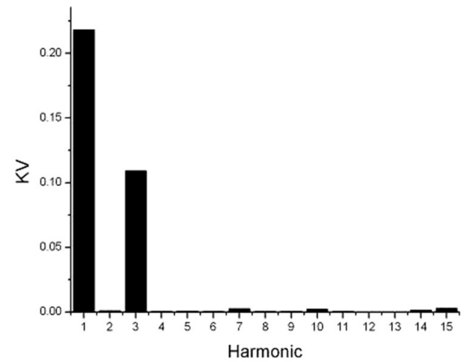

Fig. 12. Output voltage spectrum diagram

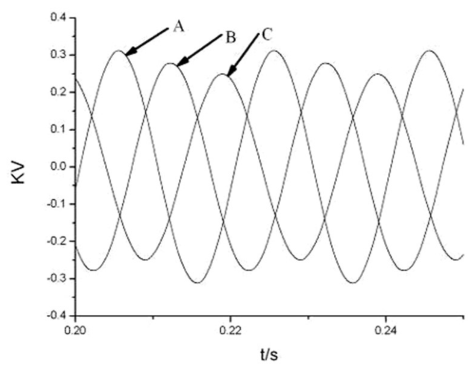

Fig. 13. Waveform diagram of three-phase unbalance simulation

4. Experimental study of VSC-IG device

VSC power disturbance generator and other power electronic devices are the synthesis of many modern technologies. Refer to Figure 14 for a depiction of the experimental device's structure.

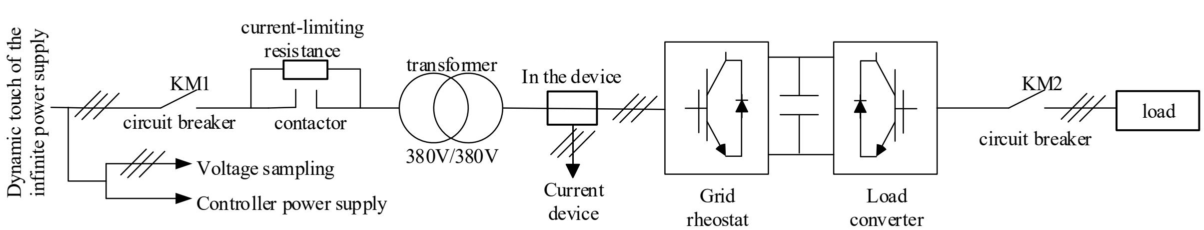

Fig. 14. Main circuit structure diagram of prototype

According to the theoretical calculation and the actual situation of the device, the technical specifications of the device are determined as shown in Table 3.

Table 3. Technical specifications of the device

Electrical parameter	Technical index
Plant capacity	30kVA
Carrying capacity	100A
Dc voltage error	±1%
Disturbance voltage control	0~112%
Maximum harmonic frequency of voltage	17

4.1. Maximum harmonic frequency of voltage

The disturbance occurs using the regular sampling PWM method, and the following disturbance waveforms are realized:

1) Voltage dip Figure 15 is the voltage dip, as shown in the diagram, starts at 220V and temporarily drops to 173V, a decrease of 21.4%, before resuming its normal level after 100ms. In the operation of power system, voltage dip may be caused by sudden failure of power grid, start-up of high-power equipment or load fluctuation of power grid. This sudden voltage reduction will directly affect the stability and safety of power equipment, especially for equipment and systems sensitive to voltage fluctuations, such as electronic equipment, computer systems, etc., may cause equipment damage or work instability.

2) Figure 16 shows the waveform of the voltage temporary rise. The voltage changes from 220V to 248V, with a temporary rise of 12.5% and a duration of 100ms. In the power system, the temporary voltage rise may be caused by the sudden reduction of grid load, generator regulation or grid voltage rebound. This sudden voltage rise may have an adverse effect on the equipment and load in the system, especially for equipment and systems that require high voltage stability, such as power electronics, communication equipment, etc., which may lead to equipment damage or system failure.

3) Voltage outages Voltage outages are the most serious power quality events. Figure 17 shows the voltage interruption waveform with a duration of 120ms. In practical applications, voltage outages can be caused by grid failures, equipment failures, or weather effects. This short but complete voltage interruption will directly lead to equipment shutdown or failure in the system, which has a serious impact on industrial production and people's livelihood facilities. Therefore, power systems need to design appropriate protection measures and emergency response strategies to minimize the impact of voltage outages on systems and equipment.

4) Harmonic injection of the third harmonic voltage of 0.5 times the base value is superimposed to the basic modulation voltage, depicted in Figure 18, facilitates the generation of three-phase unbalanced voltage outputs by adjusting the amplitudes of the respective phase modulation waves.

5) The diagram in Figure 19 portrays a three-phase voltage waveform with a noted 32.5% imbalance, and it is the stability of the DC voltage that guarantees the fidelity of the output waveform. The ability of the system to deal with the unbalanced voltage can be further understood by analyzing the waveform. In practical applications, power systems often face the situation of unbalance of the grid, such as the difference in voltage amplitude and phase, which may lead to uneven voltage distribution at the load end or cause adverse effects on power equipment. In order to effectively deal with this situation, the VSC-IG system can generate different voltage waveforms by adjusting the modulation amplitude of each phase, so as to compensate and adjust the unbalance of the power grid. The voltage waveform shown in Figure 19 reflects the operating state of the system under the condition of 32.5% imbalance. By adjusting the amplitude of the modulating wave, the system can satisfy the requirement of voltage stability and harmonic content of the load while maintaining the three-phase voltage balance. This flexible modulation technology enables VSC-IG to cope with a variety of complex grid conditions and ensure the quality and stability of the output voltage.

Figure 20 shows the voltage error diagram at the DC side when the voltage dip event as shown in Figure 20 occurs. The margin of error is noted to be within the limits of -0.2% to 0.6%, and the greatest observed change in voltage amounts to 6V, which meets the device index. The voltage error and fluctuation range indicate that the system has strong anti-disturbance ability and stable voltage performance. In the voltage dip event, the grid voltage will drop or fluctuate for a short time, which puts forward a severe test for the stable operation of power electronic devices. However, it can be seen from the error diagram that the system can still maintain high stability of DC voltage in the face of such transient interference. The error is between -0.2% and 0.6%, indicating that the system can respond quickly and adjust to suppress voltage fluctuations.

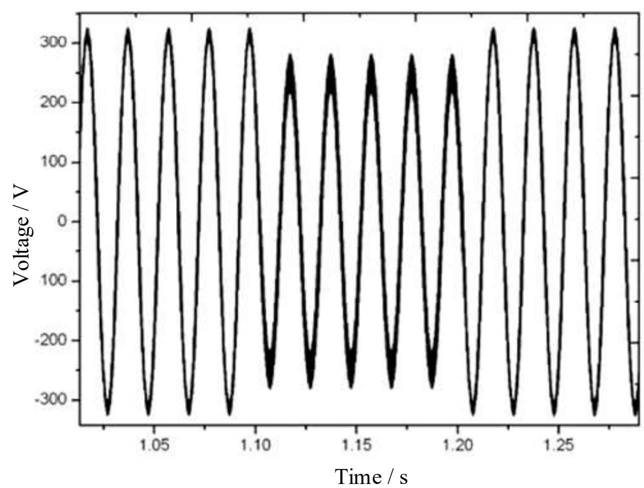

Fig. 15. Voltage dip waveform

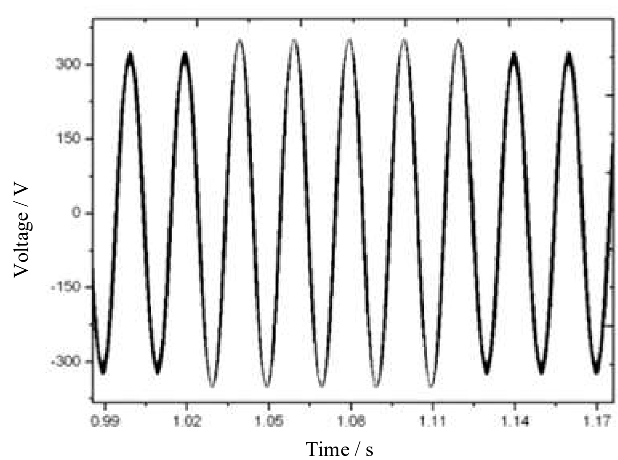

Fig. 16. Waveform of voltage temporary rise

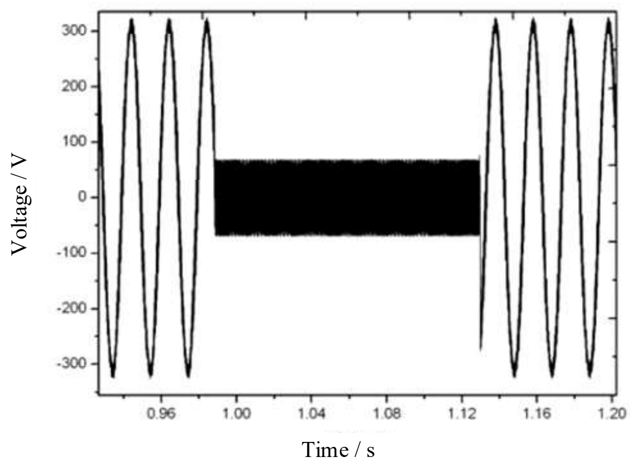

Fig. 17. Voltage interruption waveform

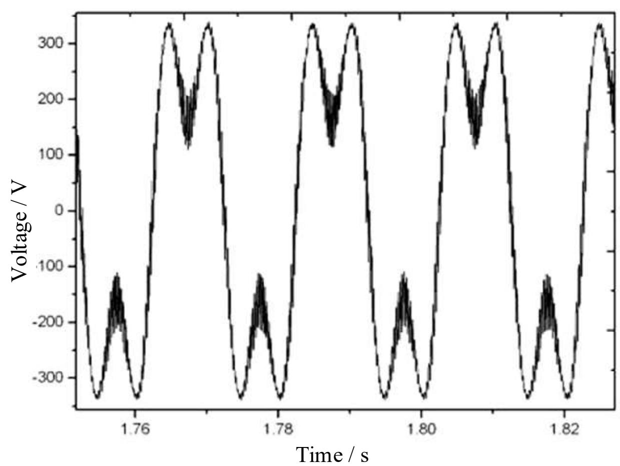

Fig. 18. Injected third harmonic waveform

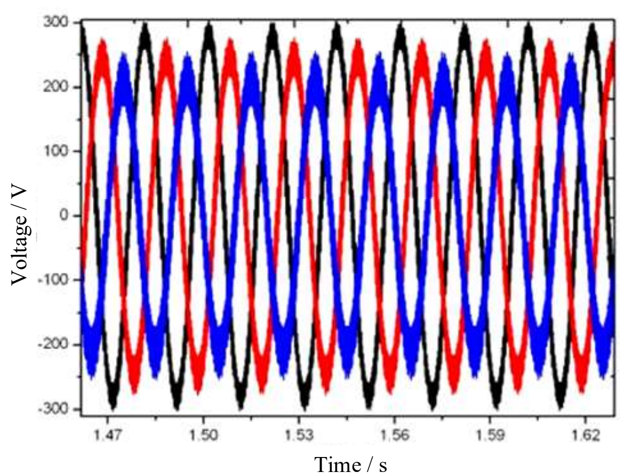

Fig. 19. Three-phase unbalanced voltage waveform

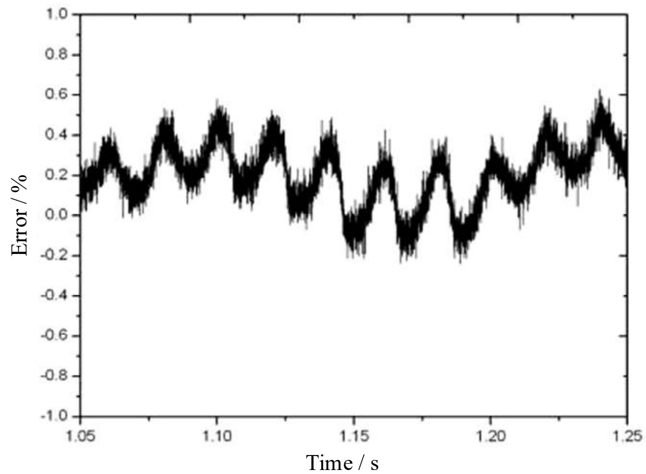

Fig. 20. DC voltage error diagram of the dip process

4.2. VSC-IG load side grid connection experiment

Figure 21 shows voltage relationship before grid connection. The VSC-IG controller detects the amplitude and phase of the grid-connected system voltage, and sets the amplitude and phase of the output voltage according to the detection results, so as to realize the grid-connected VSC-IG. Specifically, the controller first obtains real-time data of the grid voltage through sensors or acquisition devices. This data is then fed into a control algorithm in the VSC-IG system, which calculates the voltage amplitude and phase Angle to be output based on the preset grid-connection requirements and operating parameters. These calculations are then fed back to the inverter part of the VSC-IG, which controls the inverter to produce an output voltage waveform that matches the grid voltage.

In this way, VSC-IG is able to effectively synchronize with the grid and adjust its output according to grid conditions to ensure stable operation and power quality of the system. This grid-connected control strategy not only improves the response speed and stability of the system, but also helps to improve the efficiency and reliability of the power system, which is suitable for various power application scenarios, such as power electronic modulation, power grid stability control and other requirements. Using the single-phase zero crossing detection method.

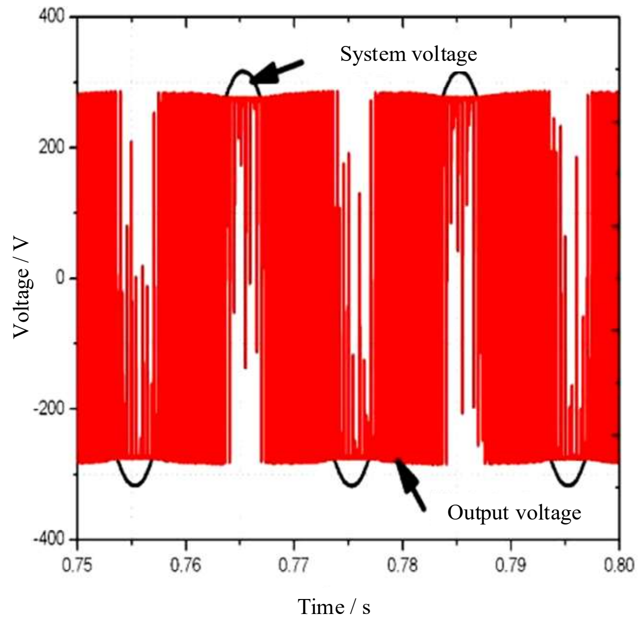

Fig. 21. Voltage relationship before grid connection

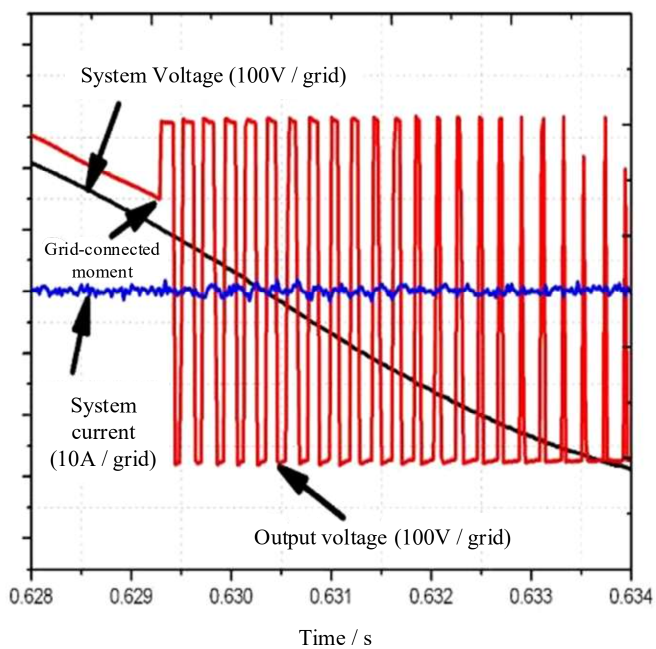

Fig. 22. Schematic diagram of each parameter during grid connection

The load side of VSC-IG was interfaced with the power grid via a 50Ω resistive link and the grid-connection experiment was carried out. Figure 22 shows the relationship between the voltage at the network side, the output voltage at the load side of VSC-IG, and the system current during grid-connection. It can be seen that when the grid is connected, the current fluctuation is small, and the load side of VSC-IG is basically attached to the grid. Set the output voltage phase to be consistent with the grid voltage, and the output voltage amplitude drops from 280V to 265V (a drop of 5.4%), and the duration is 100ms.

5. Conclusion and prospect

1) The selection of device main circuit parameters affects the operating characteristics of the equipment. Establishing numerical values for the main circuit's parameters offers essential theoretical insights for crafting the device's design.
2) The approach to managing power within the network-side converter has been carefully determined, providing a clear direction for its operational control. A double closed-loop control system for voltage control at fixed DC side is established. SPWM regular sampling method is used to realize the output of disturbance voltage, and the type of disturbance voltage can be controlled flexibly.
3) PSCAD/EMTDC software was used to establish the simulation platform of VSC power disturbance generator, and the experiment was carried out in the 30kVA physical prototype in the dynamic model laboratory. The experimental platform and relevant tools are provided for the research of power quality problems and the testing of the operating characteristics of compensation equipment under disturbed conditions.

Reference

[1] Zhang, G., Li, Z., Zhang, B., & Halang, W. A. (2018). Power electronics converters: Past, present and future. Renewable and Sustainable Energy Reviews, 81, 2028-2044.

[2] Barnes, M., Van Hertem, D., Teeuwsen, S. P., & Callavik, M. (2017). HVDC systems in smart grids. Proceedings of the IEEE, 105(11), 2082-2098.

[3] An, T., Tang, G., & Wang, W. (2017). Research and application on multi-terminal and DC grids based on VSC-HVDC technology in China. High voltage, 2(1), 1-10.

[4] Wei, B., Guerrero, J. M., Vásquez, J. C., & Guo, X. (2017). A circulating-current suppression method for parallel-connected voltage-source inverters with common DC and AC buses. IEEE Transactions on Industry Applications, 53(4), 3758-3769.

[5] Davidson, C., & Dorn, J. (2023). Power Semiconductors for LCC and VSC HVDC Valves. In High Voltage DC Transmission Systems: HVDC (pp. 1-33). Cham: Springer International Publishing.

[6] Heydari, R., Dragicevic, T., & Blaabjerg, F. (2019). High-bandwidth secondary voltage and frequency control of VSC-based AC microgrid. IEEE Transactions on Power Electronics, 34(11), 11320-11331.

[7] Gong, X., Yuan, X., Hu, J., & Wang, S. (2023). Modeling of VSC with active/reactive current excitation and internal voltage response for analyzing amplitude/frequency modulation dynamics of the grid. CSEE Journal of Power and Energy Systems.

[8] Lu, D., Wang, X., & Blaabjerg, F. (2018). Impedance-based analysis of DC-link voltage dynamics in voltage-source converters. IEEE Transactions on Power Electronics, 34(4), 3973-3985.

[9] Khobragade, M., Dalvi, H. S., & Jagtap, P. (2019). Bidirectional voltage source converter for microgrid. In Smart Technologies for Energy, Environment and Sustainable Development: Select Proceedings of ICSTEESD 2018 (pp. 29-40). Springer Singapore.

[10] Zou, G., Feng, Q., Huang, Q., Sun, C., & Gao, H. (2018). A fast protection scheme for VSC based multi-terminal DC grid. International Journal of Electrical Power & Energy Systems, 98, 307-314.

[11] Lin, S., Wang, L., Mu, D., Liu, L., Liao, K., & He, Z. (2018). Research on starting-up control strategy of VSC-HVDC system. IET Renewable Power Generation, 12(16), 1957-1965.

[12] Ghayad, M. S., Badra, N. M., Abdelaziz, A. Y., & Attia, M. A. (2019). Reactive power control to enhance the VSC-HVDC system performance under faulty and normal conditions. International Journal of Applied

Power Engineering (IJAPE), 8(2), 145-158.

[13] Wang, B., Cai, J., Du, X., & Zhou, L. (2017). Review of power semiconductor device reliability for power converters. CPSS Transactions on Power Electronics and Applications, 2(2), 101-117.

[14] Hannan, M. A., Hussin, I., Ker, P. J., Hoque, M. M., Lipu, M. H., Hussain, A., ... & Blaabjerg, F. (2018). Advanced control strategies of VSC based HVDC transmission system: Issues and potential recommendations. Ieee Access, 6, 78352-78369.

[15] Yan, X., & Zhang, W. (2019). Review of VSG control-enabled universal compatibility architecture for future power systems with high-penetration renewable generation. Applied Sciences, 9(7), 1484.

[16] Wu, S., Qi, L., Zhang, X., Zhang, B., He, Z., & Jin, M. (2023). A novel low-cost DC chopper for offshore wind VSC-HVDC system by using thyristors instead of full-control devices. IEEE Transactions on Industrial Electronics, 71(4), 3639-3649.

[17] Gao, S., Zhao, H., Gui, Y., Luo, J., & Blaabjerg, F. (2020). Impedance analysis of voltage source converter using direct power control. IEEE Transactions on Energy Conversion, 36(2), 831-840.

[18] Wang, Y., Zhou, Y., Li, D., Shao, D., Cao, K., Zhou, K., & Cai, D. (2020). The Influence of VSC–HVDC Reactive Power Control Mode on AC Power System Stability. Energies, 13(7), 1677.

[19] Wang, S., Adam, G., Ahmed, K. H., & Williams, B. (2022). Comparative evaluation of converter-based compensation schemes for VSC systems to achieve full-range active power transfer in very weak grids. Electric Power Systems Research, 210, 108135.

[20] Li, Y., Liu, H., Fan, X., & Tian, X. (2020). Engineering practices for the integration of large-scale renewable energy VSC-HVDC systems. Global Energy Interconnection, 3(2), 149-157.

[21] Khan, A., Seyedmahmoudian, M., Raza, A., & Stojcevski, A. (2021). Analytical review on common and state-of-the-art FR strategies for VSC-MTDC integrated offshore wind power plants. Renewable and Sustainable Energy Reviews, 148, 111106.

[22] Huang, W., Chen, Q., Jiang, L., Han, Y., & Qi, Y. (2018, September). New recognition method of lightning interference in long distance VSC-HVDC transmission system. In 2018 China International Conference on Electricity Distribution (CICED) (pp. 1818-1823). IEEE.